Mapping of active capable faults by high-resolution geophysical methods: examples from the central Vienna Basin

W. CHWATAL[1)], K. DECKER[2)] & K.-H. ROCH[1)]

KEYWORDS

Seismics
Vienna Basin
Geoelectrics
Active tectonics
Ground penetrating radar

[1)] Vienna University of Technology, Research Group Geophysics Gusshausstrasse 27-29, A-1040 Vienna, Austria
[2)] University of Vienna, Institute of Geological Sciences Althanstraße 14, A-1090 Vienna, Austria

Abstract

Complementary high-resolution geophysical methods (seismics, GPR with different centre frequencies, resistivity) are applied for mapping the active Markgrafneusiedel Fault in the Vienna Basin. Mapping focussed on a morphological fault scarp forming the SE boundary of the Middle Pleistocene Gänserndorf Terrace 20 km NE of the centre of Vienna. Seismic and GPR data highlight reflectors, which terminate below the morphological break of the fault scarp and thus image a fault, which dips with 55-60° to the southeast. The fault is traced from about 200 m depth up to the surface by combining reflection seismics, 40 MHz GPR data imaging the depth interval between 3 and 15 m, and 500 MHz GPR data depicting the uppermost metres. Data show an emergent fault, which clearly offsets the Pleistocene sediments. The fault is found in all sections crossing the scarp. It may be associated with a colluvial wedge depicted by the high-resolution GPR data. The location of the fault below the morphological scarp is confirmed by resistivity data, which is used to support GPR interpretations, and by a free-air gravity anomaly indicating thick unconsolidated Quaternary sediments in the hangingwall of the normal fault.

Eine Kombination von hochauflösenden geophysikalischen Methoden (Seismik, Georadar, Geoelektrik) wird für die Kartierung des aktiven Markgrafneusiedel-Bruchs im Wiener Becken angewandt. Die Aufnahmen betreffen eine störungsbedingte morphologische Stufe an der SE Grenze der mittelpleistozänen Gänserndorfer Terrasse, etwa 20 km NE des Stadtzentrums von Wien. Seismik und Georadar bilden Reflektoren ab, die unter der morphologischen Stufe enden und damit eine Störung anzeigen, die mit 55-60° nach SE einfällt. Die Störung ist von ca. 200 m Tiefe bis an die Oberfläche abgebildet. Dies wird durch die Kombination von Reflexionsseismik und Georadar erreicht, und zwar mit 40 MHz für die Abbildung des Tiefenintervalls zwischen 3 und 15 m und mit 500 MHz für die Auflösung der obersten Meter. Die Daten belegen den Versatz der pleistozänen Sedimente und zeigen eine aktive Störung, die bis an die Oberfläche reicht. An der Störung dürfte ein Keil kolluvialer Sedimente ausgebildet sein, der durch die 500 MHz Georadar-Aufnahme abgebildet wird. Die Lage der Störung unter der morphologischen Stufe wird auch durch Widerstandsdaten eingegrenzt. Zusätzliche gravimetrische Daten zeigen eine Anomalie im Bereich der Stufe, die auf mächtige quartäre Sedimente auf der abgesenkten Störungsscholle hinweisen.

1. Motivation

Recent analyses of Miocene and active tectonics in the Vienna Basin highlight a number of Miocene faults offsetting and/or delimiting Middle to Late Pleistocene deposits, which therefore are regarded active and capable generating earthquakes (Decker et al., 2005; Decker and Hinsch, this vol.; Hinsch and Decker, 2003). Identified active faults include those belonging to the major sinistral strike-slip system of the Vienna Basin transfer fault (Fig. 1; Semmering - Mitterndorf Basin - Lassee Basin – Little Carpathians; Decker & Peresson, 1998), the Leopoldsdorf fault and its continuation north of the Danube and several normal faults with minor cumulative offset such as the Markgrafneusiedel Fault in the northern central Vienna Basin (Fig. 1, 2; Hinsch et al,. 2005; this vol.). At depth the locations and geometries of many of these faults are well constrained by industry seismics and borehole data due to extensive exploration on hydrocarbons in the Vienna Basin (Kröll and Wessely, 1983; Sauer et al., 1992; Wessely, 1993). The wealth of deep subcrop data, however, strongly contrasts with the poorly constrained fault traces at the surface. The geometrical relation between faults and the uppermost sediment layers are mostly unconstrained. Such constraints, however, are needed for the reconstruction of the youngest fault history and for seismic hazard assessments including the preparation of active fault maps.

2. Geological Background of the exploration area

Geophysical fault mapping focussed on a site along a Quaternary normal fault offsetting Middle Pleistocene (Riss) alluvial gravels of the so-called Gänserndorf Terrace of the Danube in the central part of the Vienna Basin (Fig. 1, 2; Fuchs and Grill, 1984). The Middle Pleistocene terrace sediments are exposed in several gravel pits along the margin of the terrace, which show coarse to medium grained gravels with sand matrix and minor intercalations of coarse and pebbly sand. Observed sedimentary structures such as horizontal and cross stratification, imbricate pebbles and channel fill geometries are typical for braided river deposits. The local geological situation with 10 – 20 m thick Quaternary fluvial gravels overlying Miocene marl, silt and sand is typical for many suspected active faults in the vicinity of Vienna. The mapped NE-striking normal fault was first inferred by Fink (1973), who stratigraphically correlated the Middle Pleistocene gravels of the elevated part of the Gänserndorf Terrace to the Obersiebenbrunn Basin. Faulting led to a normal displacement of the top of the terrace of up to 17 m (Fig. 2). Such normal displacement of the Middle Pleistocene gravels is corroborated by the observation that gravels of the

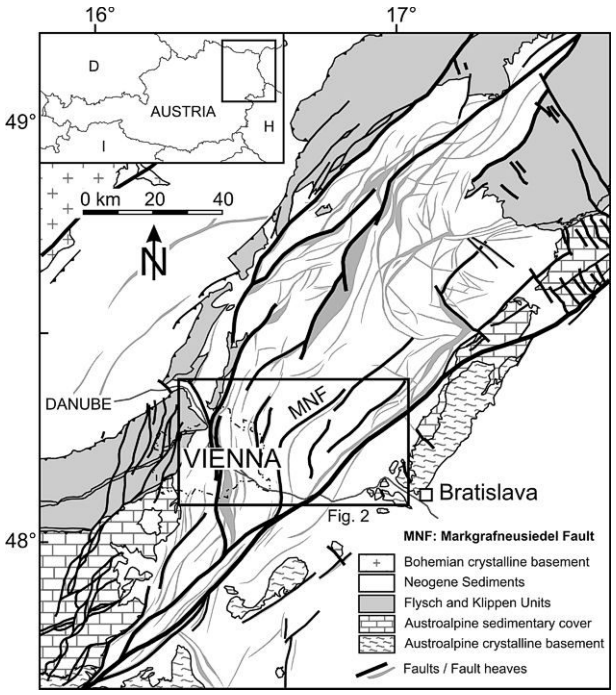

Figure 1: Tectonic sketch map of the Vienna Basin based on geological maps of Austria (1:50.000), Czecho-Slovakia (1:200.000), Fuchs and Grill (1984) and Kröll and Wessely (1993). The study area along the Markgrafneusiedel Fault is shown in Fig. 2.

Late Pleistocene (Würm) terrace locally overly the downthrown Middle Pleistocene deposits (Van Husen, pers. comm.). The fault is morphologically marked by a 10 – 17 m high fault scarp, which is traced over a distance of about 11 km. Industry seismic data show that the surface fault scarp exactly parallels a marked Miocene normal fault, which has been mapped in 3-D seismics (Peresson, pers. comm.). The fault, referred to as Markgrafneusiedel Fault, is a SE-dipping Miocene growth fault with 300 m maximum stratigraphic offset of the Late Miocene (Pannonian) strata (Hinsch et al., this vol.). Recent analyses of Quaternary sediments adjacent to the fault prove continued faulting during the Quaternary with some 40 m of Quaternary growth strata overlying the hanging wall of the fault (Decker et al., 2005). Due to the acquisition parameters of the industry seismics, however, these data does not resolve structures above 200-250 m depth including the Quaternary section.

3. Methodology

The combination of high-resolution reflection seismics and ground penetrating radar (GPR) with different acquisition parameters was used to obtain high-resolution imaging of structures and strata in the shallow subsurface. The particular goal was to achieve full image coverage of stratigraphic and structural geometries between about 250 m and <1 m depth in order to trace faults up to the surface. Both methods are capable of producing high-resolution images. It should be noted that they depict different physical properties of the subcrop, i.e. elastic parameters and changes of seismic impedance for seismics, and electromagnetic property contrasts for GPR. In order to obtain independent data for high interpretation reliability seismic and GPR profiling was combined with geoelectric and gravity measurements.

Reflection seismics for the current study uses a 96-channel OYO-DAS acquisition instrument for recording together with a hammer or a pneumatic hammer (VAKIMPAK) as energy source. The lines had geophone spacing between 3-6 m and a nominal 42-fold coverage. As reflected waves never appear as first breaks, an appropriate data acquisition and processing was applied to extract these signals from the entire wave field. The seismic data were processed with ProMAX 2D software. A standard processing sequence has been applied including automatic gain control (AGC), spiking, predictive deconvolution, bandpass filter, velocity analysis (determination of stacking velocity field), NMO-correction, CDP-stacking, and depth migration. The final result is a depth section of the underground.
Ground penetrating radar (GPR) proved as a wave method with the highest possible resolution suitable for structural exploration (e.g., Asprion et al., 1997; Reicherter and Reiss, 2001a, b; Bristow and Jol, 2003; Reiss et al., 2003). The system employs

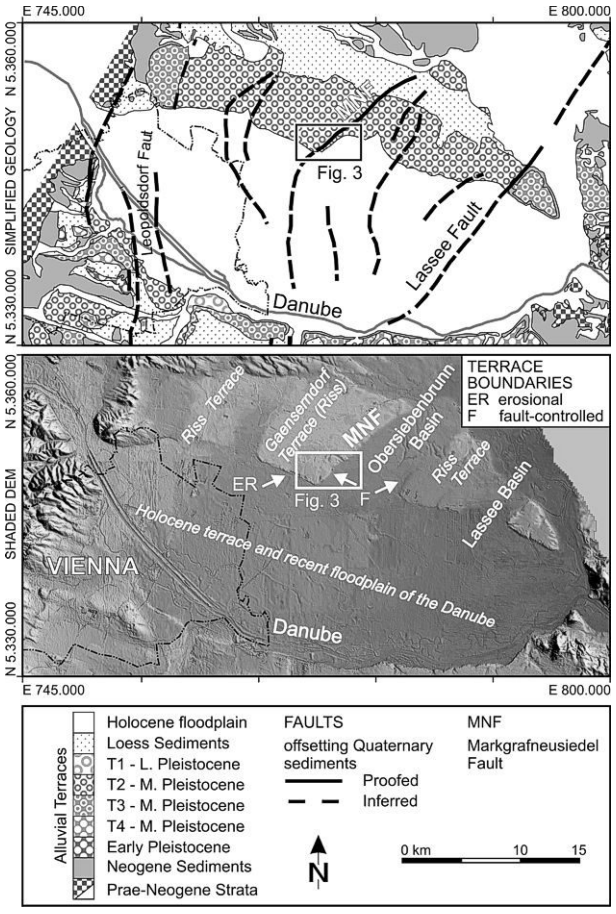

Figure 2: Geological map (a) and geomorphologic setting (b; illuminated DEM) of the central Vienna Basin in the surrounding of the Markgrafneusiedel Fault (see Fig. 1 for map location). Geophysical mapping was performed at the fault-controlled SE terrace boundary of the Gänserndorf Terrace (Middle Pleistocene, Riss). The morphological fault scarp parallels the Markgrafneusiedel Fault, which has been mapped from 3D seismic data (Hinsch et al., this vol.). Sketch map redrawn from Fuchs and Grill (1984) and Hinsch et al. (2005). Rectangles refer to the location of the geophysical basemap (Fig. 3).

electromagnetic waves in combination with the pulse echo method. A transmitter antenna radiates very short pulses (mostly centre frequencies of 10 to 1000 MHz) into the subsurface. From boundaries with electromagnetic property contrasts the pulses are reflected back to a receiver antenna at the surface. A series of scans is collected as the antennae, typically mounted with a short constant offset, are moved along a survey line. These scans form a display profile of the subsurface when positioned side by side and combined with marks indicating the current position of the antenna.

Attenuation of radar signals and thus the exploration depth is determined by the electrical conductivity of the subsurface (e.g., Smith and Jol, 1995). Attenuation increases with frequency and thus reduces exploration depth. On the other hand, the resolution increases due to the smaller wavelength. In the above mentioned frequency range resolution varies between metres and centimetres. In practice, when choosing a centre frequency, a compromise between exploration depth and resolution must be found. Within the scope of a diploma thesis (Gegenleitner, 2003) a 700 m long profile crossing the suspected fault was measured by GPR using a multiple low-frequency antenna (GSSI Model 3200 MLF) with a centre frequency of 20 MHz and a 100 MHz antenna. Recording device was a GSSI SIR 2 unit. Due to the good results of this experiment, which showed a break in a distinct boundary in a depth of about 10 meters, further investigations were carried out on a number of GPR profiles (Fig. 3). First results of measurements with centre frequencies of 20 MHz and 40 MHz were compared. Due to the portability of the multiple low-frequency antenna in the overgrown terrain the 40 MHz adjustment with a dipole length of 2.40 meters had to be preferred. The measurements were done in discrete stacking mode with a point distance of 1 or 2 meters. The main record data are: time range: 500 ns, 1024 samples/scan, 16 bits/sample, stat stack: 32.

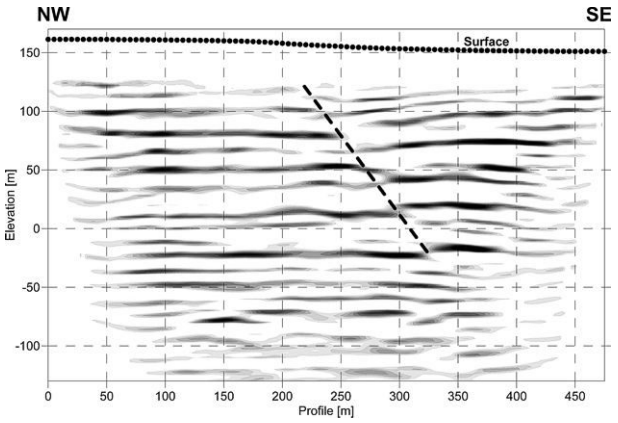

Figure 4: Seismic section and surface topography along Profile A. Discontinuous reflectors indicate a SE-dipping fault between profile m 220 (top of section) and 320 (lower part of the section). No vertical exaggeration. See Fig. 3 for location of the profile.

At profile A the low-frequency sections were combined with a further measurement using a 500 MHz antenna (time range: 120 ns, point distance 0.5 m) in order to get resolution up to the top decimetres depth. As all records were quite similar and of good quality, only moderate processing was necessary.

Geoelectric (resistivity) methods are based on the influence of resistivity of the subsurface on the propagation of electric currents. Specific resistivity particularly depends on clay content, porosity, water content and the electrical conductivity of the pore water. Resistivity methods therefore provide data on electromagnetic sediment properties, which are here used to supplement the GPR data. The array of the current electrodes and the potential electrodes along profiles follows standard geometry (e.g., Wenner). The penetration depth is controlled via the distance of the current electrodes. Geoelectric measurements for a 2D imaging of the profiles were carried out with ABEM Terrameter and a multi-electrode array with 80 electrodes and a roll along technique.

Depending upon geometry 2D images of the distribution of specific resistivity in the subsurface can be derived. In the first step the field data are presented and contoured as apparent resistivity pseudosection. These data are converted to the

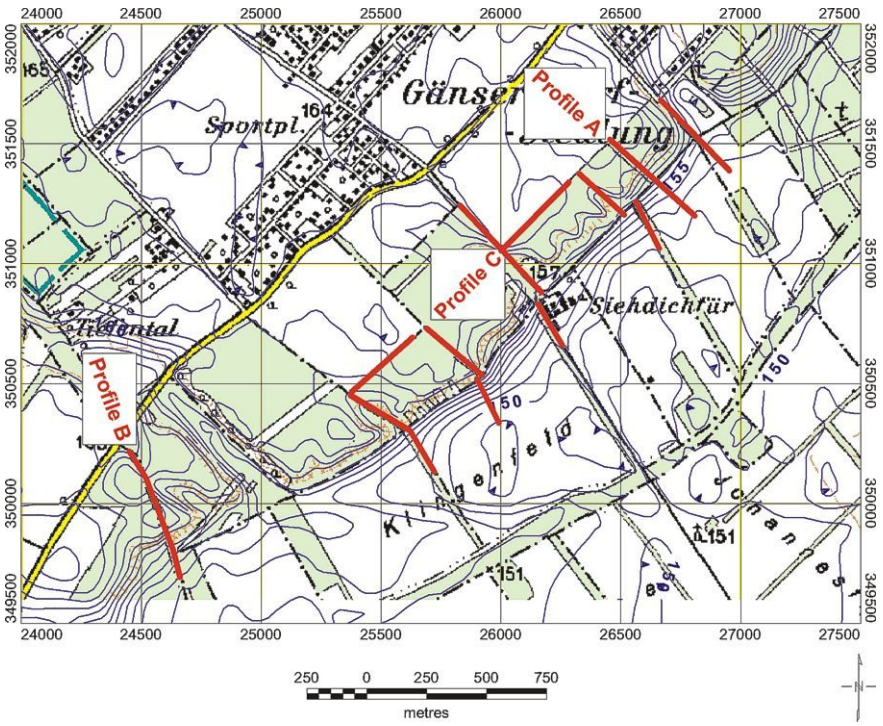

Figure 3: Locations of measured sections (GPR, seismics, resistivity) at the SE boundary of the Gänserndorf Terrace, SE of the village Gänserndorf. The field survey includes seven NW-SE-oriented cross lines and one line paralleling the fault scarp on the elevated part of the terrace.

model resistivity section, using a non-linear least squares optimization technique for the inversion subroutine (Loke and Barker, 1996). To check the calculated resistivity section, a finite-difference forward modelling subroutine is used to calculate the apparent resistivity values of the model, which then are compared with the field data.

Gravity. A gravity survey along 3 parallel lines crossing the suspected fault was carried out with a Scintrex CG3 gravity meter. Measurement point distance was 10 or 20 meters. The relative gravity values were reduced to zero height. The result is the Free-air anomaly showing a step of about 0.5 mgal in mean over the suspected fault scarp.

4. Results and interpretation

Measurements in the exploration area include 7 GPR cross lines with 300 – 400 m length perpendicular to the fault scarp (Fig. 3). Two sections (profile A and B) are covered by seismic, GPR, geoelectric and gravity measurements. On the elevated part of the scarp several cross lines were connected by a 600 m long GPR section in order to assess the geometry of the Pleistocene gravel.

The GPR sections on the elevated part of the terrace are widely consistent in depicting the Pleistocene gravels with wavy internal reflections overlying a sharp and laterally very consistent flat basal reflector at a depth between 151 and 152 m elevation (Figs. 5 to 7). Exposures of the gravels down to a depth of about 154 m in an abandoned gravel pit close to one cross line and section C (Fig. 3) allow for a straightforward interpretation of the upper part of the section. Reflector geometries such as the shallow depression of the basal reflector and onlaps on this reflector may indicate shallow fluvial channels (Fig. 7, Inline C between 120 and 300 m). By borehole evidence the basal reflector is correlated to the base of the Pleistocene gravels overlying fine-grained Miocene sediments (Sperl, 1984).

Results of the 7 measured cross lines are discussed on the examples of profile A and B. The migrated depth section of the reflection seismics A (Fig. 4) provides information for the depth range from 30 to 250 meters. Continuous flat reflectors image that both the elevated and lower part of the terrace terminate at a fault, which is traced between –20 m and 120 m elevation. The fault dips to SE with about 55° and points upwards to the morphological terrace boundary.

The results of GPR, geoelectrics and the gravity survey for the profile A are summarized in Fig. 5. The GPR section shows a prominent horizon in a depth of 8 - 10 m, which disappears below the topographic terrace boundary, i.e., in the hanging wall. This picture is similarly found in all other cross lines (compare profile B, Fig. 6). The resistivity imaging indicates, that northwest of the suspected fault gravel with high resistivities (around 2000 Ohm.m) overlay more conductive layers with 50 - 500 Ohm.m, which are interpreted as fine-grained Miocene sediments. This layering also disappears below the slope of the scarp. The data is interpreted by a downshift of the Pleistocene sediments for 10 – 20 m southeast of the fault bringing the gravel below the

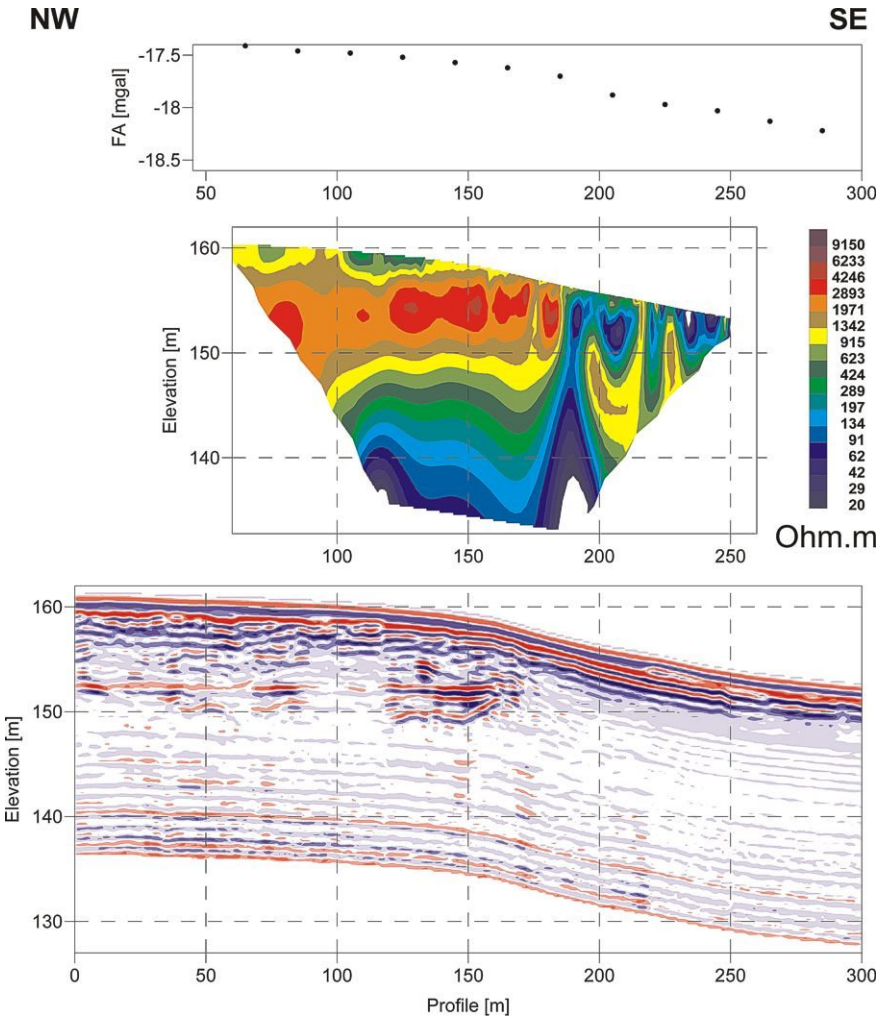

Figure 5: Free air anomaly (top), model resistivity section (centre) and 40 MHz GPR-section (below) along cross line A. In the left part of the section resistivity and GPR depict an approximately 10 m thick layer of high resistivity overlying a low-resisitvity layer. The contact is imaged as a sharp GPR reflector. The reflection pattern of the high-resistivity layer is typical for sandy gravels. The dull signals with continuous banding parallel to the surface imaged in the lower part of the section result from fine-grained shaly sediments. Note that both the resisitivity section and the GPR reflector indicate a gentle dip of the base of the high-resisitvity layer to the NW and the termination of the layer at the inferred fault near profile m 180. The location of the inferred fault coincides with the break in topography and with changing gravity values. Vertical exaggeration 1 : 4. See Fig. 3 for location of the profile.

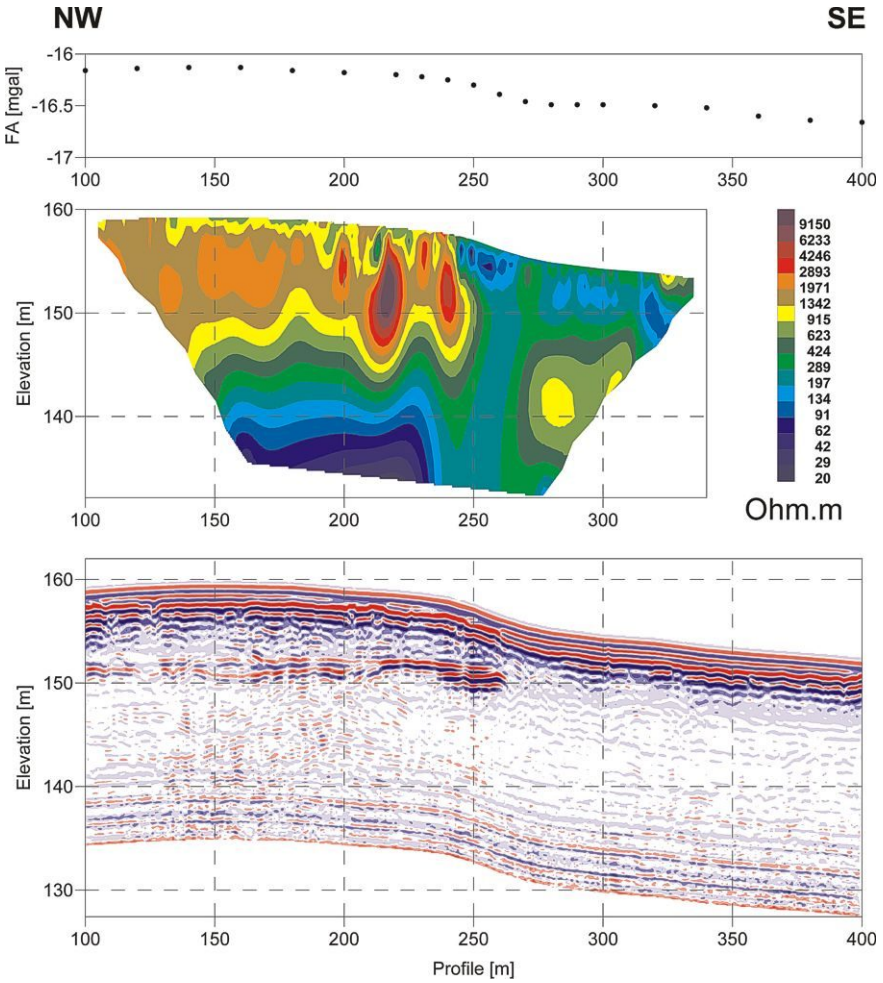

Figure 6: Free air anomaly (top), model resistivity section (centre) and 40 MHz GPR-section (below) along cross line B. Data show similar geometries as Profile A with an approximately 10 m thick high-resistivity layer overlying low-resisitvity sediments in the left part of the section. The upper layer terminates at a fault near profile m 260. Vertical exaggeration 1 : 4. See Fig. 3 for location of the profile.

groundwater table and making it invisible for both GPR and geoelectric measurements. A GPR measurement in the hangingwall of the fault with a 15 MHz antenna corresponding to an exploration depth of about 20 - 25 m also did not image indicators of a sequence comparable to that of the footwall.

In the case of using low-frequency antennae, it must be considered, that no information close to the surface can be obtained. With a frequency of 40 MHz this range goes down to approximately 3 m depth. In Fig. 5 and 6 this effect is shown by the steady signal with high amplitude at the top of the record, which was intentionally not suppressed. In order to image structures close to the surface the 40 MHz records were combined with GPR data of the 500 MHz antenna, which resolves structures in the scale of tens of centimetres. Recording focussed on the termination of the Pleistocene gravels below the morphological scarp between profile m 120 and 220 of Profile A (Fig. 8). The section depicts a well-stratified volume of sediments below the morphological slope (profile m 165 – 220), which clearly differs from the diffuse reflectivity pattern below the elevated part of the terrace (NW of profile m 165, Fig. 8). The contact between the two units dips to SE with the stratified sediments showing an onlap onto the inferred contact. The overlay of the 40 MHz and 500 MHz GPR data for profile A (Fig. 9a) shows that the discontinuity of the reflections seen in the 500 MHz data can be traced down to the termination of the reflector interpreted as base of the Pleistocene gravel. The nature of the sediments composing the wedge imaged in the 500 MHz data is not constrained by outcrop or borehole data. By its geometry, the location and the dip of its NW contact the strata are tentatively interpreted as a colluvial wedge adjacent to a surface-breaking fault.

The results of GPR, geoelectrics and gravity for profile B (Fig.6) as well as GPR data from the other cross lines are very similar to those of profile A in confirming a fault extending up into the Pleistocene strata. In all sections the fault is located at the scarp.

The interpretation is supported by the gravimetric free air anomaly which shows a step down of about 0.5 mgal from

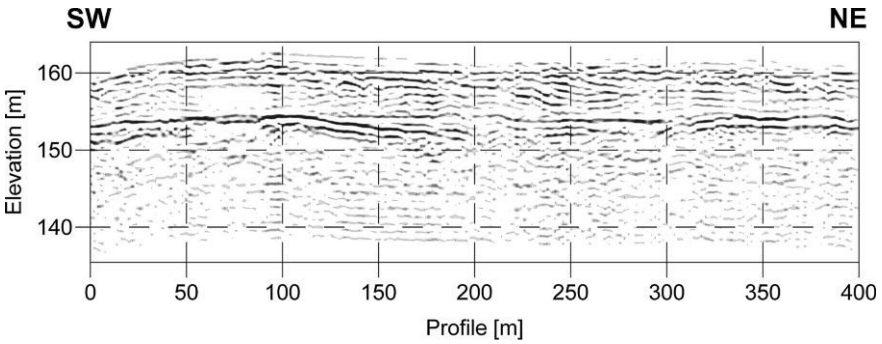

Figure 7: 40 MHz GPR-section along Profile C paralleling the fault scarp on the footwall of the Markgrafneusiedel Fault (elevated part of the Gänserndorf Terrace). The section shows a marked GPR reflector at about 150 -152 m, which is laterally consistent and traced through the entire section. Steady signals at the top of the record as seen in Figs. 5 and 6 are suppressed. The reflector is correlated to the base of Pleistocene gravels overlying Miocene fine-grained sediments. Vertical exaggeration 1 : 4. See Fig. 3 for location of the profile.

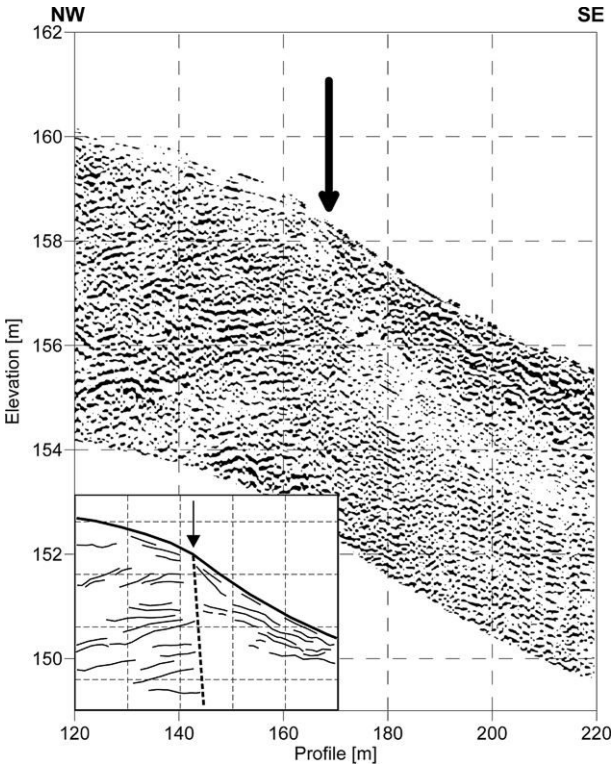

Figure 8: 500 MHz GPR-section along Profile A crossing the terrace boundary. The section shows a marked change in reflectivity around profile m 170 with little reflections near the surface to the left (NW) and thinly stratified reflective sediments to the SE (right). In the resistivity section the reflective sediments show up with low resistivity (< 100 Ohm.m, see Fig. 4). Arrow indicates the suggested outcrop trace of the fault. Vertical exaggeration 1 : 10. See Fig. 3 for location of the profile.

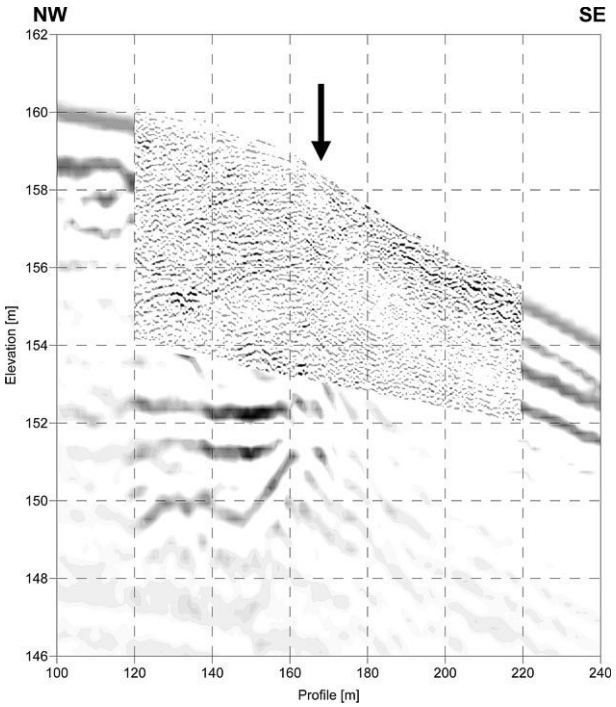

Figure 9a: Superposed images of the 40 MHz (background) and 500 MHz GPR section (overlay) along profile A. Note that the termination of the strong reflector at 152 m elevation depicted in the low-resolution 40 MHz data around profile m 170 coincides with the onset of the stratified wedge shown in the high-resolution 500 MHz data. Vertical exaggeration 1 : 10. See Fig. 3 for location of the profile.

northwest to southeast. This points out a mass deficit for the SE part of the sections. This deficit is related to the increase of the thickness of the unconsolidated Quaternary sediments overlying over-consolidated Miocene strata with higher densities. Pleistocene gravel thicknesses increase from about 10 m on the elevated part of the terrace to some 30 m in the lower part of the test site (Sperl, 1984).

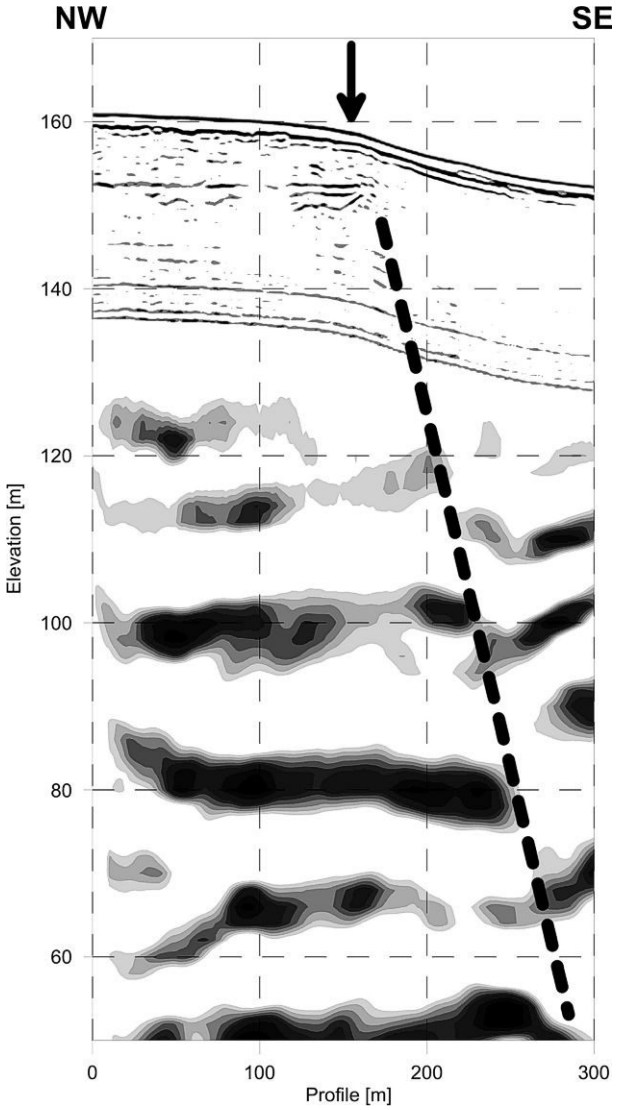

Figure 9b: Interpreted composite image of the seismic section and the 40 MHz GPR data, Profile A. The fault mapped in the seismic data continues up section to the termination of the GPR reflector at 152 m elevation. The position of the fault at the surface coincides with the topographic break. Vertical exaggeration 1 : 5.

5. Conclusions

Combined seismic and GPR data in profiles crossing the southeastern morphological boundary of the Gänserndorf Terrace highlight reflectors, which terminate below the morphological break of the fault scarp and thus image a fault, which dips with 55-60° to the southeast (Fig. 9b). The fault is traced from about 200 m depth up to the surface by combining reflection seismics, 40 MHz GPR data imaging the depth interval

between 3 and 15 m, and 500 MHz GPR data depicting the uppermost 4-6 m. Data show an emergent (capable) fault, which clearly offsets the Pleistocene sediments. The fault trace is found in all sections crossing the scarp and it may be associated with a colluvial wedge depicted by the high-resolution GPR data (Fig. 8). The location of the fault below the morphological scarp is confirmed by additional resistivity data, which were especially used to support GPR interpretations, and by free-air anomaly indicating thick unconsolidated Quaternary sediments in the hangingwall of the normal fault.

The example of the Markgrafneusiedel Fault scarp shows, that the combination of shallow reflection seismics and GPR is highly suitable for mapping faults at the test site, which is regarded typical for several other suspected fault scarps and active faults in the Vienna Basin (Decker et al., 2005). GPR centre frequencies of 40 and 500 MHz, turned out best applicable for profiling the site. Data provide continuous images of stratigraphic and tectonic geometries between the upper limit of industry seismic data and the surface. GPR records with 500 MHz proved particularly suitable for high-resolution images of the uppermost 4-6 m. Independently derived resistivity sections support the reliability of the data, which is of fundamental importance for locating active faults, assessing the geometrical relations between faults and young sediments and for the preparation of further exploration including trenching. The test site also shows, that within the scope of required accuracy, economic geophysical data acquisition is possible.

Acknowldedgements

Research on active fault scarps was supported by the Austrian Academy of Sciences, the FP5 project ENTEC (HPRN-CT-2000-00053) and the Hochschuljubiläumsstiftung der Stadt Wien (H-1427/2002). The authors thank Helmuth Sölva and Klaus Reicherter for their constructive and thorough reviews.

References

Asprion, U., Reicherter, K. and Meschede, M. 1997. Das Bodenradar und seine Anwendung zur Erkennung tektonischer Strukturen: ein Beispiel aus dem Freudenstädter Graben (Schwarzwald, Südwestdeutschland). Jahresberichte und Mitteilungen des oberrheinischen geologischen Vereins, Neue Folge, 79, 111-124.

Bristow, C.S. and Jol, H.M. 2003. Ground Penetrating Radar: Applications in Sediments. Geological Society London Special Publication, 211, 338 pp.

Decker, K. and Peresson, H. 1998. Miocene to present-day tectonics of the Vienna Basin transform fault. In: Links between the Alps and the Carparthians, XVI Congress of the Carparthian-Balkan Geological Association, Geologische Bundesanstalt, Wien, pp. 33-36.

Decker, K., Peresson, H., and Hinsch, R. 2005. Active tectonics and Quaternary basin formation along the Vienna Basin Transform fault. Quaternary Science Reviews, 24, 307-322.

Fink, J. 1973. Zur Morphogenese des Wiener Raumes. Zeitschrift für Geomorphologie, Supplement 17, 91-117.

Fuchs, W., and Grill, R. 1984. Geologische Karte von Wien und Umgebung 1:200.000, Geologische Bundesanstalt, Wien.

Gegenleitner, R. 2003. Anwendung von Georadarmessungen zur Untersuchung von neotektonischen Vorgängen im Wiener Becken. Diploma Thesis, Vienna University of Technology, Vienna.

Gegenleitner, R. Hinsch, R., Brückl, E., Decker, K. and Roch, K.H. 2003. Locating neotectonic faults by GPR and reflection seismics, EGS - AGU - EUG – Joint Assembly Nice, 2003, Geophysical Research Abstracts, 5, 09050.

Hinsch, R. and Decker, K. 2003. Do seismic slip deficits indicate an underestimated earthquake potential along the Vienna Basin Transform Fault System? Terra Nova, 15, 343-349.

Hinsch, R., Decker, K. and Peresson, H. 2005. 3-D seismic interpretation and structural modelling in the Vienna Basin: implications for Miocene to recent kinematics. Austrian Journal of Earth Sciences, this. Vol.

Hinsch, R., Decker, K. and Wagreich, M. 2005. 3-D Mapping of segmented active faults in the southern Vienna Basin. Quaternary Science Reviews, 24, 321-336.

Kröll, A. and Wessely, G. 1993. Wiener Becken und angrenzende Gebiete. Geologische Themenkarte der Republik Österreich 1:200.000. Geologische Bundesanstalt, Wien.

Loke, M.H. and Barker, R.D. 1996. Practical techniques for 3D resistivity surveys and data inversion. Geophysical Prospecting, 44, 499-523.

Reicherter, K. and Reiss, S. 2001a. The Carboneras Fault Zone (southeastern Spain) revisited with Ground Penetrating Radar - Quaternary structural styles from high-resolution images. Geologie en Mijnbow / Netherlands Journal Earth Sciences, 80, 11-20.

Reicherter, K. and Reiss, S. 2001b. Active faults in the Cubillas reservoir area mapped by 3D-ground penetrating radar imaging (northeastern Granada Basin, southern Spain). Zentralblatt Geologie Paläontologie, Teil 1, 2002, 167-179.

Reiss, S., Reicherter, K. and Reuther, C.-D. 2003. Visualization and characterization of active normal faults and associated sedimentary structures by high-resolution ground penetrating radar (GPR). In: C.S. Bristow and H.M. Jol (Editors), Ground Penetrating Radar in Sediments. Geological Society London Special Publication, 211, 247-255.

Sauer, R., Seifert, P. and Wessely, G. 1992. Guidebook to excursions in the Vienna Basin and the adjacent Alpine-Carpathian thrustbelt in Austria. Mitteilungen der geologischen Gesellschaft, 85, 1-264.

Smith, D.G., and Jol, H.M. 1995. Ground penetrating radar: antenna frequencies and maximum probable depths of penetration in Quaternary sediments. Journal Applied Geophysics, 33, 93-100.

Sperl, H. 1984. Marchfeld: Oberkante des maßgeblichen Grundwasserstauers und Lage der Bohrungen. Unpublished Map, Österr. Donaukraftwerke AG, Vienna.

Wessely, G. 1993. Der Untergrund des Wiener Beckens. In: F. Brix, and O. Schulz (Editors), Erdöl und Erdgas in Österreich, pp. 249-280.

Received: 21. February 2005
Accepted: 19. April 2005

W. CHWATAL[1)], K. DECKER[2)] & K.-H. ROCH[1)]

[1)] Vienna University of Technology, Research Group Geophysics Gusshausstrasse 27-29, A-1040 Vienna, Austria

[2)] University of Vienna, Institute of Geological Sciences Althanstraße 14, A-1090 Vienna, Austria